BIOCHEMISTRY
including biophysical chemistry & molecular biology

Article

pubs.acs.org/biochemistry

Effect of Thiazole Orange Doubly Labeled Thymidine on DNA Duplex Formation

Yasumasa Kimura,* Takeshi Hanami, Yuki Tanaka, Michiel J. L. de Hoon, Takahiro Soma, Matthias Harbers, Alexander Lezhava, Yoshihide Hayashizaki, and Kengo Usui

RIKEN Omics Science Center (OSC), RIKEN Yokohama Institute, 1-7-22 Suehiro-cho, Tsurumi-ku, Yokohama, Kanagawa 230-0045, Japan

Supporting Information

ABSTRACT: Nucleic acid oligonucleotides are widely used in hybridization experiments for specific detection of complementary nucleic acid sequences. For design and application of oligonucleotides, an understanding of their thermodynamic properties is essential. Recently, exciton-controlled hybridization-sensitive fluorescent oligonucleotides (ECHOs) were developed as uniquely labeled DNA oligomers containing commonly one thymidine having two covalently linked thiazole orange dye moieties. The fluorescent signal of an ECHO is strictly hybridization-controlled, where the dye moieties have to intercalate into double-stranded DNA for signal generation. Here we analyzed the hybridization thermodynamics of ECHO/DNA duplexes, and thermodynamic parameters were obtained from melting curves of 64 ECHO/DNA duplexes measured by ultraviolet absorbance and fluorescence. Both methods demonstrated a substantial increase in duplex stability ($\Delta\Delta G^\circ_{37} \sim -2.6 \pm 0.7$ kcal mol^{-1}) compared to that of DNA/DNA duplexes of the same sequence. With the exception of T·G mismatches, this increased stability was mostly unaffected by other mismatches in the position opposite the labeled nucleotide. A nearest neighbor model was constructed for predicting thermodynamic parameters for duplex stability. Evaluation of the nearest neighbor parameters by cross validation tests showed higher predictive reliability for the fluorescence-based than the absorbance-based parameters. Using our experimental data, a tool for predicting the thermodynamics of formation of ECHO/DNA duplexes was developed that is freely available at http://genome.gsc.riken.jp/echo/thermodynamics/. It provides reliable thermodynamic data for using the unique features of ECHOs in fluorescence-based experiments.

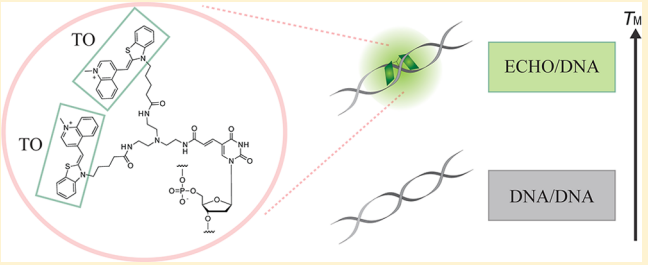

Over the past four decades, nucleic acid hybridization techniques have been widely used for the detection of specific complementary nucleic acid sequences in a variety of applications, including Southern and Northern blots, real-time PCR (polymerase chain reaction), FISH (fluorescence in situ hybridization), and microarrays.[1−6] Many forms of modified nucleic acids and nucleic acid analogues have been developed for those hybridization techniques that use different labels, depend on certain structural features, or have modified nucleic acid backbones.[7−12] Signal specificity largely depends on high signal-to-noise ratios. The specificity of hybridization can be improved by stabilizing hybridization to the target sequence and/or by destabilizing hybridization to nontarget sequences. Locked nucleic acid (LNA)[11] and peptide nucleic acid (PNA)[12] are nucleic acid analogues broadly used for this purpose. The background signal depends strongly on the nature of the fluorescent dye used in the hybridization and is often difficult to suppress.[13−15]

Exciton-controlled hybridization-sensitive fluorescent oligonucleotide (ECHO) is a modified DNA oligomer usually containing one thymidine covalently labeled by two paired thiazole orange molecules[16−18] [T^E (Figure 1A)]. In single-stranded DNA, the fluorescence emission of ECHOs is strongly suppressed by an excitonic interaction between the two dye moieties.[19] When an ECHO binds to a complementary nucleic acid molecule, a strong emission is observed after the excitonic interaction between the two dye moieties is disrupted and each dye independently intercalates into the DNA duplex (Figure 1B). This photophysical process allows ECHOs to function as unique "sequence-specific dyes" in hybridization-based approaches having high signal-to-noise ratios because of the strong background suppression in the single-stranded oligonucleotide. For multiplex detection, ECHOs have been synthesized using different derivatives of thiazole orange, all of which show suppression of the background signal.[20] ECHOs have already been utilized in different applications where they can function both as a primer and as a hybridization probe. For example, during isothermal amplification reactions using the SmartAmp2 amplification process, fluorescently labeled amplicons were obtained by sequence-specific incorporation of ECHOs (called "exciton primers" in ref 21). Furthermore, because of the hybridization-dependent signal, ECHOs were

Received: March 1, 2012
Revised: June 27, 2012
Published: July 5, 2012

   dx.doi.org/10.1021/bi300293d | *Biochemistry* 2012, 51, 6056−6067

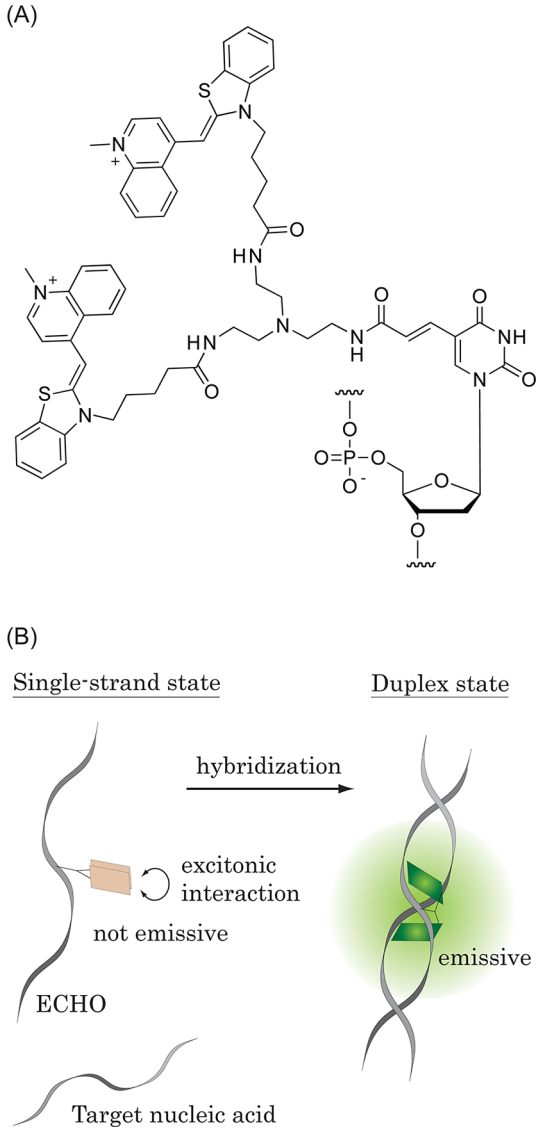

Figure 1. Properties of an ECHO. (A) Chemical structure of thymidine covalently labeled by two paired thiazole orange molecules (T^E). (B) Mechanism of ECHO-mediated signals. The excitonic interaction between the two dye moieties is disrupted once each dye moiety independently intercalates into double-stranded DNA.

used for direct in vivo detection of miRNA in living cells.[20] During such experiments, it was noticed that ECHOs have a higher binding affinity for complementary DNA or RNA than standard DNA oligomers. The binding is probably stabilized by the two thiazole orange moieties in the ECHO.[18] Thiazole orange moieties in ECHOs are structurally similar to individual thiazole orange and homodimeric thiazole orange dyes, possessing cationic charges and aromatic surfaces (see Figure 1A). They interact with oligonucleotides by ionic interaction between the cationic dye and negatively charged DNA,[22] and a base stacking interaction between the aromatic surfaces of thiazole orange and the bases in DNA.[23−25]

Although ECHOs gained attention as hybridization probes and labeled primers, no comprehensive analysis of their thermodynamics has been performed. For ECHO design, a better understanding of key features, for instance, the potential roles of sequence dependence, length dependence, and the effects of mismatch base pairing, is essential. These questions are best approached by developing folding and hybridization thermodynamic models. Nearest neighbor models have previously been used for sequence-dependent thermodynamic models for DNA/DNA,[26−32] RNA/RNA,[33−35] and DNA/RNA[31,36,37] duplexes, as well as modified nucleotides.[38−41] Ultraviolet absorbance has commonly been used in melting curve analysis to obtain thermodynamic parameters, but recently, high-throughput fluorescence monitoring was also used in thermodynamic studies.[42−47] Such approaches open interesting applications for future use of ECHO-derived fluorescence in melting curve analysis.

Here we used a set of 64 ECHO/DNA pairs to obtain a complete set of nearest neighbor parameters for ECHO/DNA duplex formation. The results from ultraviolet absorbance and fluorescence measurements allowed us to prepare a nearest neighbor model that was evaluated by cross validation tests. The nearest neighbor model can be utilized for future ECHO design and analysis.

MATERIALS AND METHODS

Materials. High-performance liquid chromatography-purified ECHOs (product name "Eprimer") were purchased from DNAFORM K.K. (Yokohama, Japan). High-performance liquid chromatography-purified DNA oligomers were purchased from Sigma-Aldrich Japan K.K. (Tokyo, Japan).

Absorbance Melting Curve Procedure. Ultraviolet absorbance-based melting experiments were performed in a 300 μL volume using a Beckman (Fullerton, CA) single-beam DU800 spectrometer with the Micro Tm Analysis accessory, a Beckman High Performance Peltier Controller, and 1 cm path length quartz cuvettes. ECHO and DNA oligomers were dissolved in a buffer containing 980 mM NaCl, 10 mM Na_2HPO_4, and 0.1 mM Na_2EDTA (pH 7, adjusted with H_3PO_4) at a concentration of 1 μM. One ECHO/DNA duplex was melted at concentrations of 0.5, 2, and 4 μM to spot-validate that $\Delta H°$ and $\Delta S°$ are concentration-independent. Samples were heated to 95 °C, maintained at 95 °C for 5 min, and cooled to room temperature. Melting curves were acquired from 8 to 95 °C, with the temperature increasing in 0.5 °C increments, waiting for 8 min at the first step and for 30 s at each step thereafter. Ultraviolet absorbance was acquired at each temperature increment. The ultraviolet absorbance melting curves of DNA/DNA and ECHO/DNA duplexes were measured at 260 nm. The melting curves were observed at least three times for each duplex. The thermodynamic parameters of each melting curve were calculated in triplicate and then averaged for each duplex.

Fluorescence Melting Curve Procedure. Real-time fluorescent monitoring was performed in 96-well plates in a volume of 25 μL using a Bio-Rad Laboratories (Foster City, CA) CFX96 system and the same buffer conditions described above. Samples were heated to 95 °C, maintained at 95 °C for 5 min, and cooled to room temperature. Excitation and detection wavelengths of the fluorescence were 510 and 530 nm, respectively. Fluorescence melting curves were measured at 530 nm by scanning from 4 to 95 °C, with the temperature increasing in 0.5 °C increments, waiting for 30 s at the first step and for 5 s at each step thereafter. The fluorescence melting curves were observed at least three times for each ECHO/DNA duplex. Logarithmic values of measured fluorescence were used for further analysis to compare them with the ultraviolet absorbance melting profiles described by the Lambert−Beer law. The thermodynamic parameters of each fluorescence

dx.doi.org/10.1021/bi300293d | Biochemistry 2012, 51, 6056−6067

melting curve were calculated and then averaged for each ECHO/DNA duplex using three independent measurements.

Melting Curve Data Analysis. The melting curves Y measured by the ultraviolet absorbance at 260 nm and measured by the logarithmic fluorescence at 530 nm were analyzed using a two-state thermodynamic model. The melting curve Y at temperature T is given by

$$Y(T) = \alpha(l_{ds}T - b_{ds}) + (1 - \alpha)(l_{ss}T - b_{ss}) \quad (1)$$

where l_{ds} and l_{ss} are the slopes and b_{ds} and b_{ss} the intercepts of the double-stranded (ds) and single-stranded (ss) state baselines, respectively.[48,49] l_{ds}, b_{ds}, l_{ss}, and b_{ss} were obtained by linear fitting of the baselines. α is the fraction of the total DNA strands found in double-stranded form.

The equilibrium constant describing the two-state hybridization of DNA is given by

$$K(T) = \frac{\alpha C_T/2}{[(1 - \alpha)C_T/2]^2} = \frac{2\alpha}{(1 - \alpha)^2 C_T} \quad (2)$$

where C_T is the total single-strand concentration. Solving the equation for α and choosing the physically realizable root, we have

$$\alpha(T) = \frac{1 + C_T K - \sqrt{1 + 2C_T K}}{C_T K} \quad (3)$$

The temperature-dependent equilibrium constant is given by

$$K(T) = \exp\left[-\frac{\Delta G^\circ_T}{R(T + 273.15)}\right] = \exp\left[-\frac{\Delta H^\circ}{R(T + 273.15)} + \frac{\Delta S^\circ}{R}\right] \quad (4)$$

where the changes in enthalpy (ΔH°) and entropy (ΔS°) are both negative, as they refer to the change upon hybridization. R is the universal gas constant. Substitutions of these equations into eq 1 give Y as a function of l_{ds}, l_{ss}, b_{ds}, b_{ss}, C_T, ΔH°, and ΔS°. C_T was set at 1 μM, and l_{ds}, l_{ss}, b_{ds}, and b_{ss} were obtained by fitting the baselines. This leaves ΔH° and ΔS° to be fitted to the measured melting curve Y as described above.

With the fitted values for ΔH° and ΔS°, the Gibbs free energy at temperature T (ΔG°_T) is given by

$$\Delta G^\circ_T = \Delta H^\circ - (T + 273.15)\Delta S^\circ \quad (5)$$

ΔG°_{37} and ΔG°_{60}, the Gibbs free energies at 37 and 60 °C, respectively, were calculated in this study, because 37 °C is the standard temperature used in thermodynamic studies and 60 °C is the incubation temperature for most isothermal amplifications. Moreover, 60 °C is in range of the annealing temperatures used in many PCR setups.

The melting temperature T_M is given by

$$T_M = \frac{\Delta H^\circ}{\Delta S^\circ + R \ln(C_T/4)} - 273.15 \quad (6)$$

Curve fitting and other calculations described here were performed by using the statistical computing environment R version 2.12.[50]

Calculation of Incremental Thermodynamic Parameters. We assumed that the thermodynamic parameters of ECHO/DNA duplexes are comprised of a contribution of reference DNA/DNA duplexes and an incremental effect by a $\mathbf{T^E}$ substitution. For example, the enthalpy of an ECHO/DNA duplex is given by

$$\Delta H^\circ_{(ECHO/DNA)} = \Delta H^\circ_{(DNA/DNA)} + \Delta\Delta H^\circ \quad (7)$$

The incremental thermodynamic parameters of a $\mathbf{T^E}$ substitution, $\Delta\Delta H^\circ$, $\Delta\Delta S^\circ$, $\Delta\Delta G^\circ_{37}$, $\Delta\Delta G^\circ_{60}$, and ΔT_M, were calculated as the changes in ΔH°, ΔS°, ΔG°_{37}, ΔG°_{60}, and T_M, respectively. The thermodynamic parameters of reference DNA/DNA duplexes used here were predicted by using the hybrid-2s.pl program in the UNAfold software package[51] under the salt condition used in the experiments (program parameters set to 1000.2 mM Na^+ and 0 mM Mg^{2+}). The thermodynamic parameters for several DNA/DNA duplexes were experimentally measured, and we concluded that the difference from the predicted values was acceptable.

Calculation of Nearest Neighbor Parameters. We modeled the incremental thermodynamic parameters as the effect of a set of three nucleotides including $\mathbf{T^E}$ ($N\mathbf{T^E}N$), which can be decomposed as the combination of two nearest neighbors ($N\mathbf{T^E}$ and $\mathbf{T^E}N$). For example, the incremental enthalpy of ECHO/DNA, $\Delta\Delta H^\circ$, is given by

$$\Delta\Delta H^\circ \cong \Delta\Delta H^\circ_{N\mathbf{T^E}N} = \Delta\Delta H^\circ_{N\mathbf{T^E}} + \Delta\Delta H^\circ_{\mathbf{T^E}N} \quad (8)$$

Multiple linear regression analysis using singular value decomposition described previously[33] was applied separately to the sets of $\Delta\Delta H^\circ$, $\Delta\Delta S^\circ$, $\Delta\Delta G^\circ_{37}$, and $\Delta\Delta G^\circ_{60}$ to yield the incremental nearest neighbor thermodynamic parameters of the dinucleotides. The variance σ^2 estimated from three replicates was used as a weighting factor. For example, the set of incremental enthalpies ($\Delta\Delta H^\circ_{N\mathbf{T^E}}$ and $\Delta\Delta H^\circ_{\mathbf{T^E}N}$) were calculated by minimizing the error-weighted squares of the residual χ^2

$$\chi^2 = \sum_{N_1}\sum_{N_2} \frac{\left\{\Delta\Delta H^\circ_{N_1\mathbf{T^E}N_2(obs)} - \left[\Delta\Delta H^\circ_{N_1\mathbf{T^E}(pred)} + \Delta\Delta H^\circ_{\mathbf{T^E}N_2(pred)}\right]\right\}^2}{\sigma^2_{N_1\mathbf{T^E}N_2}} \quad (9)$$

where (obs) and (pred) denote observed and predicted values, respectively.

The nearest neighbor model was constructed using 64 11-mer ECHO/DNA duplexes containing all possible trinucleotides: 16 for full match (NAN) and 48 for mismatches (NCN, NGN, and NTN). To evaluate the model, we performed cross validation tests in which the observed data set was divided into a training set and a test set. For each division, 4 of 16 ECHO/DNA pairs were selected for the test as they contained all nonredundant dinucleotides. The 12 remaining pairs were used for training. We considered all 24 possible division patterns of the observed data set.

The singular-value decomposition analysis and the cross validation test described here were performed by using the statistical computing environment R version 2.12.[50]

RESULTS AND DISCUSSION

Sequence Design. To obtain thermodynamic parameters for the formation of ECHO/DNA duplexes, we designed a set of 16 different ECHOs (Figure 2), where the nucleotides flanking $\mathbf{T^E}$ were systematically altered for analysis of the nearest neighbor parameters. Because we assumed the two-state melting model in our melting curve analysis, the basic DNA sequence (5′-CCATTGCTACC-3′) was taken from past studies[26,40] that also employed the same two-state melting model. In the sequence, the fifth nucleotide was replaced with

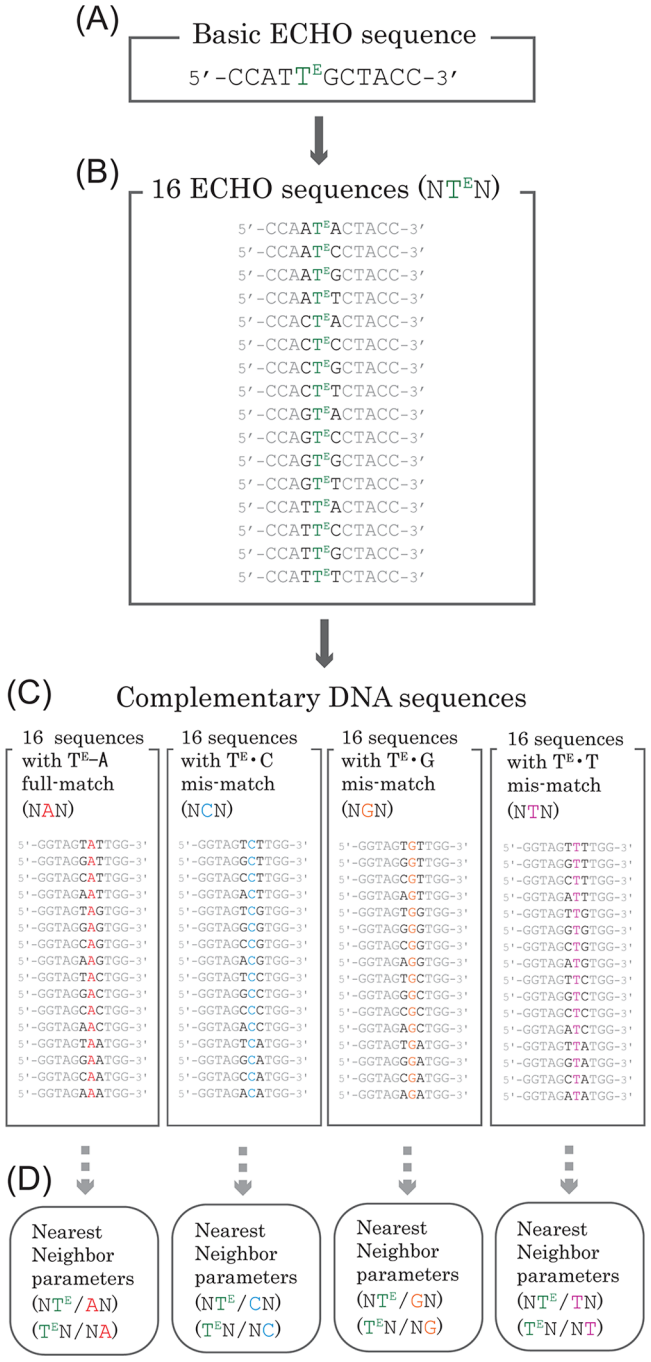

Figure 2. Oligonucleotides prepared for this study. (A) Sequence of a basic ECHO. (B) Sequences of 16 ECHOs. (C) Sequences of 64 cDNA oligomers. (D) Nearest neighbors considered for the thermodynamic model.

$\mathbf{T^E}$, designing the basic ECHO sequence (5′-CCAT-$\mathbf{T^E}$GCTACC-3′). All 16 possible combinations of trinucleotides around $\mathbf{T^E}$ (N$\mathbf{T^E}$N) were designed by altering the two proximal nucleotides. Complementary DNA sequences were designed for the analysis of the thermodynamics of all full matches and all possible mismatches to $\mathbf{T^E}$. Mismatched bases C, G, and T were introduced at the nucleotide position complementary to the $\mathbf{T^E}$ position, where the full-matching base is A. In total, all 64 possible trinucleotide combinations in DNA, including 16 for full matches (NAN) and 48 mismatches (NCN, NGN, and NTN), were designed. The two-state assumption in melting considers only the formation of a complete double-stranded duplex and the fully separated single-stranded stage of the oligonucleotides. Using the hybrid-ss-min program in the UNAfold software package,[51] we therefore computationally predicted secondary structures of each oligonucleotide that may interfere with the two-state assumption under the salt conditions intended for use in our experiments (program parameters set to 1000.2 mM Na^+ and 0 mM Mg^{2+}). None of the designed DNA sequences had secondary structures with negative free energies at 37 °C. Therefore, we concluded that the effects of secondary structures are negligible, and the two-state assumption is applicable for all the designed sequences used in this study.

Thermodynamic Effect of $\mathbf{T^E}$. Melting curves of the 64 ECHO/DNA duplexes were first measured by the changes in the ultraviolet absorbance at 260 nm over the entire range from 8 to 95 °C. From the melting curves, thermodynamic parameters were calculated as indicated in Materials and Methods (Table S1 of the Supporting Information). In brief, ΔH° and ΔS° were obtained by curve fitting to the melting curves, and ΔG°_{37}, ΔG°_{60}, and T_M were calculated from ΔH° and ΔS°. The incremental thermodynamic effect of $\mathbf{T^E}$ substitution ($\Delta\Delta H^\circ$, $\Delta\Delta S^\circ$, $\Delta\Delta G^\circ_{37}$, $\Delta\Delta G^\circ_{60}$, and ΔT_M) was calculated as the difference between ECHO/DNA and DNA/DNA duplexes with the same composition (Figure 3).

In accordance with a previous report,[18] the observed $\Delta\Delta G^\circ_{37}$, $\Delta\Delta G^\circ_{60}$, and ΔT_M showed a clear increase in the stability of duplex formation in all the ECHO/DNA duplexes; on average $\Delta\Delta G^\circ_{37} \sim -2.6 \pm 0.7$ kcal mol^{-1}, a level equal to that of a combination of two nearest neighbors in DNA/DNA Watson–Crick base pairing.[26,28,30] The underlying $\Delta\Delta H^\circ$ and $\Delta\Delta S^\circ$ values varied substantially, but consistent with previous reports,[40,52,53] a remarkably high correlation (Pearson r = 0.998; $P < 10^{-74}$) between enthalpy and entropy (Figure 4), known as enthalpy–entropy compensation,[54] was observed. It seems that a tighter binding (larger $-\Delta\Delta H^\circ$) is accompanied by a larger loss of degrees of freedom (larger $-\Delta\Delta S^\circ$) in a compensatory manner, resulting in a relatively small binding free energy, $\Delta\Delta G^\circ$.

The observed thermodynamics grouped by full-match (NAN) and mismatch (NCN, NGN, and NTN) sequences are summarized in Table 1. On one hand, the full-match group (NAN) showed an increase in both enthalpy and entropy (positive $\Delta\Delta H^\circ$ and $\Delta\Delta S^\circ$). This increase implies the contribution of the entropy was greater than that of the enthalpy. On the other hand, in the mismatch sequences, the averaged thermodynamics showed a decrease in enthalpy (negative $\Delta\Delta H^\circ$), which suggested that the contribution of the enthalpy was greater than that of the entropy. In both cases, the stability of the duplex could be caused by base stacking and ionic interaction between the two thiazole orange dyes and DNA discussed above.

Most unnatural nucleotides have hybridization thermodynamics different from those of natural DNA, either increasing or decreasing the stability and specificity of hybridization. LNA and PNA are known to increase the specificity and stability of hybridization and are used as therapeutic and diagnostic tools.[12,55,56] LNA substitution of one base slightly stabilizes DNA/DNA duplex formation with a $\Delta\Delta G^\circ_{37}$ of approximately −0.6 kcal mol^{-1} at ∼1 M Na^+.[40] PNA/DNA hybrids are more stable than DNA/DNA duplexes of the same base composition with a $\Delta\Delta G^\circ_{25}$ of approximately −2.6 kcal mol^{-1} for an 11-mer oligonucleotide at ∼0.1 M Na^+. The incremental stability of a

dx.doi.org/10.1021/bi300293d | Biochemistry 2012, 51, 6056–6067

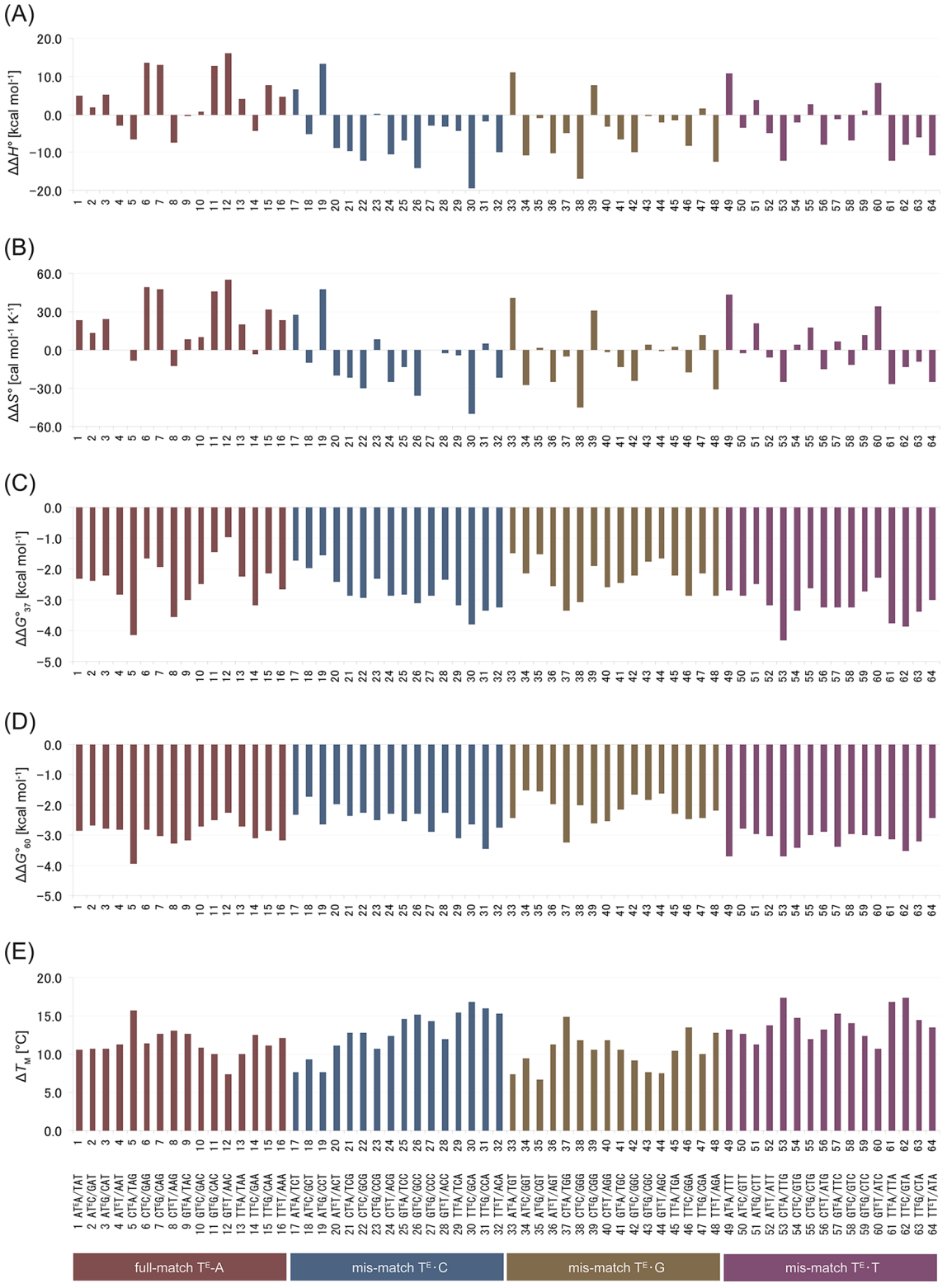

Figure 3. Incremental thermodynamic effect of $\mathbf{T^E}$ obtained from absorbance measurements: (A) $\Delta\Delta H°$, (B) $\Delta\Delta S°$, (C) $\Delta\Delta G°_{37}$, (D) $\Delta\Delta G°_{60}$, and (E) ΔT_M. Trinucleotide sequences around $\mathbf{T^E}$ are given.

PNA/DNA hybrid is proportional to the PNA oligonucleotide length.[53] One $\mathbf{T^E}$ substitution in DNA as used in the ECHOs in this study had nearly the same duplex stability with DNA ($\Delta\Delta G°_{37} \sim -2.4$ kcal mol^{-1} at ~1 M Na^+) as found for an 11-mer PNA/DNA hybrid. Whereas the stability of PNA/DNA hybrids directly increases with the length of the hybrid, ECHOs can be designed with multiple $\mathbf{T^E}$ substitutions to stepwise enhance their binding stability.

Predictive Nearest Neighbor Parameters for the Incremental Thermodynamic Effects. For prediction of thermodynamics of ECHO/DNA duplex formation, two nearest neighbor ($\mathbf{NT^E}$ and $\mathbf{T^EN}$) parameters for the

dx.doi.org/10.1021/bi300293d | *Biochemistry* 2012, 51, 6056−6067

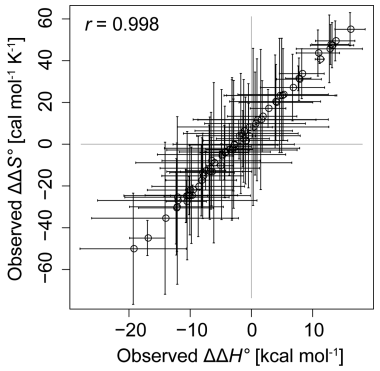

Figure 4. Relationship of $\Delta\Delta H^\circ$ vs $\Delta\Delta S^\circ$ obtained from absorbance measurements.

incremental thermodynamic effects of $\mathbf{T^E}$ substitution were obtained through multiple linear regression. To evaluate predictive accuracy, we performed cross validation tests in which 12 of 16 sequence pairs in each of four match types (NAN, NCN, NGN, and NTN) were used for training and the remaining ones were used for testing. The predicted thermodynamic parameters were compared with the observed parameters by calculating the Pearson correlation r between them. There were no significant correlations for $\Delta\Delta H^\circ$ and $\Delta\Delta S^\circ$, but a positive correlation was observed for $\Delta\Delta G^\circ_{37}$ [r = 0.30; $P < 10^{-10}$ (Figure 5A)] and particularly for $\Delta\Delta G^\circ_{60}$ [r = 0.72; $P < 10^{-64}$ (Figure 5B)]. These positive correlations suggest the incremental free energies were predicted well by the nearest neighbor parameters, indicating that the effects of $\mathbf{T^E}$ substitution are sequence-dependent. The correlations for $\Delta\Delta G^\circ_T$ at other temperatures are shown in Figure 5C. The correlations as a function of temperature followed a curve with a peak (r = 0.74; $P < 10^{-67}$) around 66 °C. The shape of the curve suggests a high reliability of the prediction of $\Delta\Delta G^\circ_T$ around 60 °C. Finally, the free energy $\Delta G^\circ_{T(\mathrm{ECHO/DNA})}$ of the ECHO/DNA duplex was calculated as the sum of the $\Delta G^\circ_{T(\mathrm{DNA/DNA})}$ of the reference DNA/DNA and the incremental $\Delta\Delta G^\circ_T$ [$\Delta G^\circ_{T(\mathrm{ECHO/DNA})} = \Delta G^\circ_{T(\mathrm{DNA/DNA})} + \Delta\Delta G^\circ_T$]. The correlations of free energy $\Delta G^\circ_{T(\mathrm{ECHO/DNA})}$ were higher [for ΔG°_{37}, r = 0.84 and $P < 10^{-104}$, and for ΔG°_{60}, r = 0.96 and $P < 10^{-205}$ (Figure 5D–F)] than the incremental $\Delta\Delta G^\circ_T$, where $\Delta\Delta G^\circ_T$ shows also a hill-shaped curve over the entire temperature range (Figure 5F). The final nearest neighbor parameters for the incremental effects using 64 11-mer sequences are listed in Table 2. Standard deviations of the nearest neighbor parameters tended to have larger $\Delta\Delta G^\circ_{37}$ values than $\Delta\Delta G^\circ_{60}$ values. We speculate that this tendency is due to errors at low temperatures before the melting curve transition phase. Analyzing additional duplexes with low melting temperatures may improve the accuracy at low temperatures.

Mismatch Effect on ECHO/DNA Duplex Formation. To investigate how ECHOs can discriminate between mismatches, we compared the hybridization free energies of the full matches and mismatches on the same sequence. The differences in the free energies at 60 °C between full-match $\mathbf{T^E}$-A pairs and $\mathbf{T^E}$·C, $\mathbf{T^E}$·G, and $\mathbf{T^E}$·T mismatches were calculated as indicators of a mismatch effect ($\Delta_{\mathrm{full/mis}}\Delta G^\circ_{60}$) and visualized in a heat map (Figure 6A). As a reference, the same indicators were calculated for T·C, T·G, and T·T compared to T-A in the reference DNA/DNA duplexes (Figure 6B). The effects of mismatches to $\mathbf{T^E}$ varied depending on the proximal bases but were overall at a level [$\Delta_{\mathrm{full/mis}}\Delta G^\circ_{60(\mathrm{ECHO/DNA})} \sim -2.5 \pm 0.6$ kcal mol^{-1}] similar to that of the mismatches to the T in DNA/DNA duplexes [$\Delta_{\mathrm{full/mis}}\Delta G^\circ_{60(\mathrm{DNA/DNA})} \sim -2.2 \pm 0.6$ kcal mol^{-1}]. However, there was a substantial difference for T·G mismatches where $\Delta_{\mathrm{full/mis}}\Delta G^\circ_{60}$ was larger for a $\mathbf{T^E}$·G mismatch [$\Delta_{\mathrm{full/mis}}\Delta G^\circ_{60(\mathrm{ECHO/DNA})} \sim -2.3 \pm 0.4$ kcal mol^{-1}] than a T·G mismatch [$\Delta_{\mathrm{full/mis}}\Delta G^\circ_{60(\mathrm{DNA/DNA})} \sim -1.5 \pm 0.3$ kcal mol^{-1}] in a DNA/DNA duplex. The larger effect for a $\mathbf{T^E}$·G mismatch could be advantageous for developing mutation detection assays. The hydrolytic deamination of 5-methylcytosines causes frequent T·G mismatches in genomic DNA, which can be converted into G to A or C to T mutations.[57]

Relationship between Fluorescence and Absorbance Melting Profiles. Because an ECHO fluoresces upon hybridization,[16,17] we confirmed whether the absorbance melting profiles correlate with the fluorescence melting profiles obtained for the same oligonucleotides. Fluorescence-based

Table 1. Average Thermodynamic Parameters for ECHO/DNA Duplex Formation

group	ΔH° (kcal mol^{-1})	ΔS° (cal mol^{-1} K^{-1})	ΔG°_{37} (kcal mol^{-1})	ΔG°_{60} (kcal mol^{-1})	T_M (°C)
full-match					
$\mathbf{T^E}$-A	−76.0 ± 6.8	−200 ± 20.6	−14.0 ± 0.9	−9.4 ± 0.8	57.2 ± 3.6
mismatch					
$\mathbf{T^E}$·C	−67.9 ± 6.9	−185 ± 20.6	−10.6 ± 0.8	−6.3 ± 0.7	42.5 ± 3.7
$\mathbf{T^E}$·G	−71.1 ± 5.8	−192 ± 17.4	−11.6 ± 1.0	−7.1 ± 1.0	46.8 ± 4.4
$\mathbf{T^E}$·T	−72.0 ± 6.6	−195 ± 19.5	−11.6 ± 1.0	−7.1 ± 0.9	46.8 ± 4.0
all					
$\mathbf{T^E}$·N	−71.8 ± 7.0	−193 ± 19.9	−11.9 ± 1.6	−7.5 ± 1.4	48.3 ± 6.7

group	$\Delta\Delta H^\circ$ (kcal mol^{-1})	$\Delta\Delta S^\circ$ (cal mol^{-1} K^{-1})	$\Delta\Delta G^\circ_{37}$ (kcal mol^{-1})	$\Delta\Delta G^\circ_{60}$ (kcal mol^{-1})	ΔT_M (°C)
full-match					
$\mathbf{T^E}$-A	3.9 ± 7.3	20.4 ± 21.3	−2.4 ± 0.8	−2.9 ± 0.4	11.4 ± 1.8
mismatch					
$\mathbf{T^E}$·C	−5.5 ± 7.9	−9.2 ± 24.0	−2.7 ± 0.6	−2.5 ± 0.4	12.7 ± 2.9
$\mathbf{T^E}$·G	−4.2 ± 7.3	−6.1 ± 22.5	−2.3 ± 0.6	−2.2 ± 0.5	10.3 ± 2.3
$\mathbf{T^E}$·T	−3.1 ± 6.9	0.2 ± 21.0	−3.1 ± 0.5	−3.1 ± 0.3	13.9 ± 2.0
all					
$\mathbf{T^E}$·N	−2.2 ± 8.1	1.3 ± 24.6	−2.6 ± 0.7	−2.7 ± 0.5	12.1 ± 2.6

dx.doi.org/10.1021/bi300293d | Biochemistry 2012, 51, 6056−6067

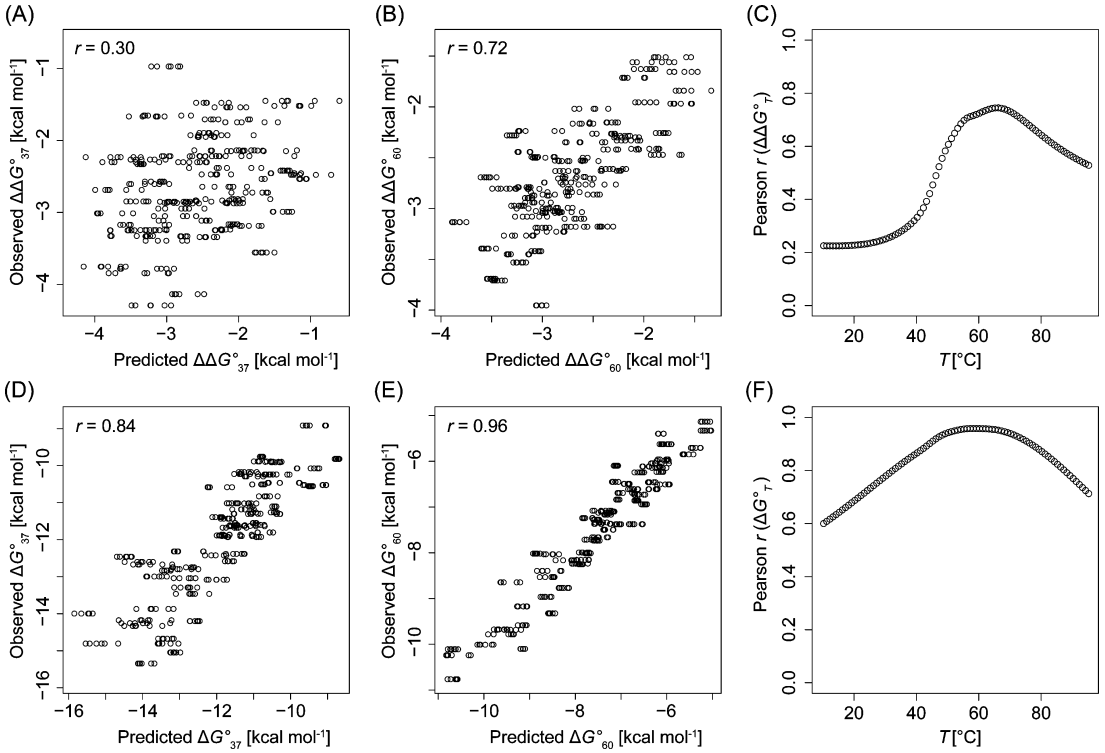

Figure 5. Evaluation of the nearest neighbor thermodynamic parameters obtained from absorbance measurements. Comparison between the predicted and observed $\Delta\Delta G^\circ_{37}$ (A), $\Delta\Delta G^\circ_{60}$ (B), ΔG°_{37} (D), and ΔG°_{60} (E) values. (C and F) Pearson correlation r of the predicted vs the observed $\Delta\Delta G^\circ_T$ (C) and ΔG°_T (F) over the temperature range.

thermodynamic parameters were obtained for all 64 11-mer ECHO/DNA duplexes (Tables S2 and S3 and Figures S1−S3 of theSupporting Information), and the fluorescence-based data were calculated by the same procedures outlined above for the analysis of the absorbance data. The relationship between fluorescence and absorbance melting profiles was investigated by calculating the Pearson correlation r comparing their thermodynamic parameters. The comparison between the fluorescence- and absorbance-based parameters showed a low correlation for enthalpy ΔH° (r = 0.40, and P < 0.01) and entropy ΔS° (r = 0.25, and P < 0.05) (Figure 7A,B). Fluorescence-based enthalpy ΔH° and entropy ΔS° tended to be lower than their absorbance-based counterparts, with average decreases of −12 kcal mol^{-1} and −34 cal mol^{-1} K^{-1}, respectively. These decreases derived from a short transition phase in the fluorescence melting curves. The 260 nm absorption captures separation of all hydrogen bonds, whereas fluorescence captures disruption of hydrogen bonds around $\mathbf{T^E}$. We speculate that capturing a few base pairs around the $\mathbf{T^E}$ resulted in a shorter transition phase compared to capturing all the base pairs. In contrast to ΔH° and ΔS°, high correlations for ΔG°_{37} (r = 0.94; $P < 10^{-29}$) and ΔG°_{60} (r = 0.98; $P < 10^{-41}$) were observed between the fluorescence- and absorbance-based parameters (Figure 7C,D). These high correlations suggest that the absorbance- and fluorescence-based thermodynamics are compatible with each other in terms of hybridization stability. The apparent average increases in stability for fluorescence-based ΔG°_{37}, ΔG°_{60}, and T_M compared to the absorbance-based values were found to be −1.3 kcal mol^{-1}, −0.5 kcal mol^{-1}, and 3.4 °C, respectively. This tendency may have been caused by the nature of the fluorescence of the ECHO, or the $\mathbf{T^E}$ positioned in the middle dissociated later compared to bases positioned at terminal ends. The effects of $\mathbf{T^E}$ in other positions need to be further investigated.

The nearest neighbor parameters derived from the fluorescence melting curves were also calculated (Table S4 of the Supporting Information) and evaluated using the same procedures that were applied to the absorbance melting curves (Figure 8). The evaluation of the fluorescence-based nearest neighbor parameters showed high correlations of $\Delta\Delta G^\circ_T$ (for $\Delta\Delta G^\circ_{37}$, r = 0.79 and $P < 10^{-82}$; for $\Delta\Delta G^\circ_{60}$, r = 0.80 and $P < 10^{-86}$) between predictions and observations (Figure 8A−C). The comparison between the fluorescence- and absorbance-based nearest neighbor parameters showed a low correlation for $\Delta\Delta G^\circ_{37}$ [r = 0.27; P < 0.2 (Figure 7E)] and a high correlation for $\Delta\Delta G^\circ_{60}$ [r = 0.69; $P < 10^{-4}$ (Figure 7F)]. This tendency in the correlation coefficients is very similar to that in the absorbance-based nearest neighbor $\Delta\Delta G^\circ_{37}$ (r = 0.30) and $\Delta\Delta G^\circ_{60}$ (r = 0.72) (Figure 5A,B). Therefore, we speculate that errors from the absorbance-based nearest neighbor parameters in panels A and B of Figure 5 are mainly causing the tendency shown in panels E and F of Figure 7. Overall, the fluorescence-based nearest neighbor parameters showed a higher predictive reliability (Figure 8A−C) than the absorbance-based parameters (Figure 5A−C), underlining the potential merits of the use of fluorescence for ECHO thermodynamics studies and fluorescence-based applications.

Prediction Tool for ECHO Analysis and Design. On the basis of the obtained final nearest neighbor parameters outlined above using absorption and fluorescence data together with unified DNA/DNA nearest neighbor parameters of SantaLucia,[27] we established a tool for predicting the thermodynamics of ECHO/DNA duplex formation. In our experiments, the Na^+ concentration was set to 1 M to directly compare our data with previously reported nucleic acid thermodynamic parame-

dx.doi.org/10.1021/bi300293d | Biochemistry 2012, 51, 6056−6067

Table 2. Obtained Nearest Neighbor Parameters

nearest neighbor (5′ to 3′/5′ to 3′)	$\Delta\Delta H^\circ$ (kcal mol^{-1})	$\Delta\Delta S^\circ$ (cal mol^{-1} K^{-1})	$\Delta\Delta G^\circ_{37}$ (kcal mol^{-1})	$\Delta\Delta G^\circ_{60}$ (kcal mol^{-1})
full match				
AT^E/AT	−1.8 ± 1.7	−1.2 ± 3.0	−1.4 ± 0.4	−1.3 ± 0.2
CT^E/AG	1.4 ± 1.3	8.4 ± 2.2	−1.2 ± 0.4	−1.6 ± 0.3
GT^E/AC	10.6 ± 1.3	34.6 ± 2.3	−0.5 ± 0.4	−1.4 ± 0.2
TT^E/AA	−0.1 ± 1.4	3.9 ± 2.3	−1.3 ± 0.4	−1.4 ± 0.2
T^{E}A/TA	−5.4 ± 1.6	−11.0 ± 2.7	−1.8 ± 0.4	−1.5 ± 0.2
T^{E}C/GA	6.7 ± 1.5	24.4 ± 2.5	−0.9 ± 0.4	−1.3 ± 0.3
T^{E}G/CA	8.3 ± 1.3	29.0 ± 2.2	−0.8 ± 0.4	−1.2 ± 0.2
T^{E}T/AA	0.4 ± 1.3	3.4 ± 2.3	−0.9 ± 0.4	−1.7 ± 0.2
mismatch T^E·C				
AT^E/CT	5.4 ± 1.3	19.1 ± 2.3	−0.7 ± 0.2	−0.9 ± 0.2
CT^E/CG	−8.1 ± 1.3	−21.2 ± 2.2	−1.4 ± 0.5	−1.2 ± 0.2
GT^E/CC	−4.5 ± 2.0	−9.7 ± 3.5	−1.3 ± 0.3	−1.3 ± 0.3
TT^E/CA	−4.4 ± 1.6	−8.3 ± 2.9	−1.9 ± 0.4	−1.7 ± 0.3
T^{E}A/TC	−1.3 ± 1.3	−0.3 ± 2.1	−1.5 ± 0.3	−1.4 ± 0.3
T^{E}G/CC	6.7 ± 1.6	25.0 ± 2.9	−1.0 ± 0.4	−1.7 ± 0.3
T^{E}C/GC	−10.3 ± 1.4	−28.5 ± 2.6	−1.3 ± 0.3	−1.0 ± 0.2
T^{E}T/AC	−6.6 ± 1.9	−16.3 ± 3.3	−1.6 ± 0.3	−1.0 ± 0.4
mismatch T^E·G				
AT^E/GT	2.4 ± 1.0	9.4 ± 1.8	−0.6 ± 0.3	−0.7 ± 0.2
CT^E/GG	−2.5 ± 1.4	−3.1 ± 2.4	−1.5 ± 0.5	−1.5 ± 0.3
GT^E/GC	1.2 ± 1.3	6.8 ± 2.3	−1.4 ± 0.2	−0.8 ± 0.3
TT^E/GA	−5.0 ± 1.6	−11.3 ± 2.7	−1.2 ± 0.4	−1.5 ± 0.3
T^{E}A/TG	8.3 ± 1.1	29.9 ± 1.8	−1.0 ± 0.2	−1.6 ± 0.2
T^{E}C/GG	−12.4 ± 1.3	−35.3 ± 2.3	−1.5 ± 0.4	−0.9 ± 0.2
T^{E}G/CG	6.1 ± 1.6	22.7 ± 2.7	−0.7 ± 0.5	−0.8 ± 0.2
T^{E}T/AG	−6.0 ± 1.3	−15.6 ± 2.2	−1.5 ± 0.4	−1.1 ± 0.3
mismatch T^E·T				
AT^E/TT	0.7 ± 1.2	7.1 ± 2.1	−1.4 ± 0.3	−1.5 ± 0.2
CT^E/TG	−0.7 ± 1.3	3.6 ± 2.3	−1.7 ± 0.3	−1.6 ± 0.2
GT^E/TC	6.5 ± 1.6	23.1 ± 2.8	−0.8 ± 0.3	−1.5 ± 0.3
TT^E/TA	−6.7 ± 1.6	−16.0 ± 2.8	−2.2 ± 0.3	−1.8 ± 0.2
T^{E}A/TT	4.3 ± 1.6	18.6 ± 2.8	−1.9 ± 0.4	−2.0 ± 0.3
T^{E}C/GT	−2.9 ± 1.3	−3.6 ± 2.3	−1.6 ± 0.3	−1.5 ± 0.3
T^{E}G/CT	2.6 ± 1.5	11.5 ± 2.7	−1.0 ± 0.4	−1.4 ± 0.2
T^{E}T/AT	−4.2 ± 1.2	−8.8 ± 2.1	−1.6 ± 0.3	−1.5 ± 0.2

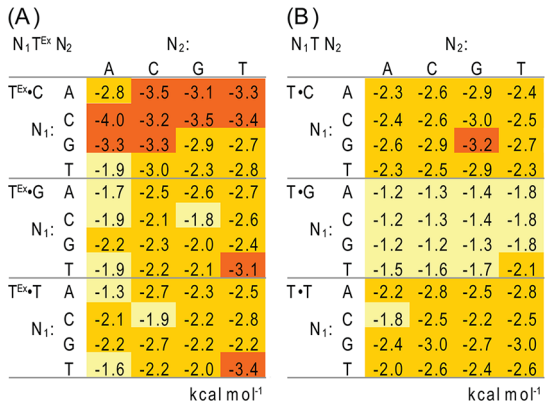

Figure 6. Effect of mismatches on ΔG°_{60}. Differences in free energies at 60 °C ($\Delta_{full/mis}\Delta G^\circ_{60}$) between full match T^E-A and mismatches T^E·C, T^E·G, and T^E·T were calculated and visualized in heat maps based on absorbance measurements for (A) ECHO/DNA duplexes and (B) DNA/DNA duplexes. Red indicates larger changes, whereas yellow indicates smaller effects on $\Delta_{full/mis}\Delta G^\circ_{60}$.

ters.[26,28,30,33,36,37,40] However, in PCR and isothermal DNA amplification, much lower concentrations of Na^+ and other reagents such as Mg^{2+}, deoxynucleotide triphosphates (dNTPs), and dimethyl sulfoxide (DMSO) are commonly used. In living cells, concentrations of K^+, Na^+, and Mg^{2+} vary among cell types and conditions. The influences of those cations and reagents on nucleic acid thermodynamics have been investigated.[27,38,58,59] They showed that higher concentrations of cations cause the lower stability of duplex formation in its dependence on oligonucleotide length. Such analysis provided information for the rough estimation of ECHO/DNA thermodynamics under different solution conditions. We employed the salt corrections of SantaLucia[27] to predict ECHO/DNA duplex stability under different conditions. The resulting prediction tool provides ΔH°, ΔS°, ΔG°_T, and T_M values for input sequences of a given ECHO/DNA duplex, where the user can assign individual values for the Na^+ and Mg^{2+} concentrations. The tool is freely available online at http://genome.gsc.riken.jp/echo/thermodynamics/.

To evaluate our online tool and the final nearest neighbor parameters, we synthesized three additional 20-mer ECHOs to analyze possible effects of oligonucleotide length on ECHO/DNA thermodynamics (Table 3). The predictive duplex stability of the 20-mer sequences was calculated by our tool, and the predicted and observed $\Delta\Delta G^\circ_{37}$ and $\Delta\Delta G^\circ_{60}$ values for

dx.doi.org/10.1021/bi300293d | Biochemistry 2012, 51, 6056−6067

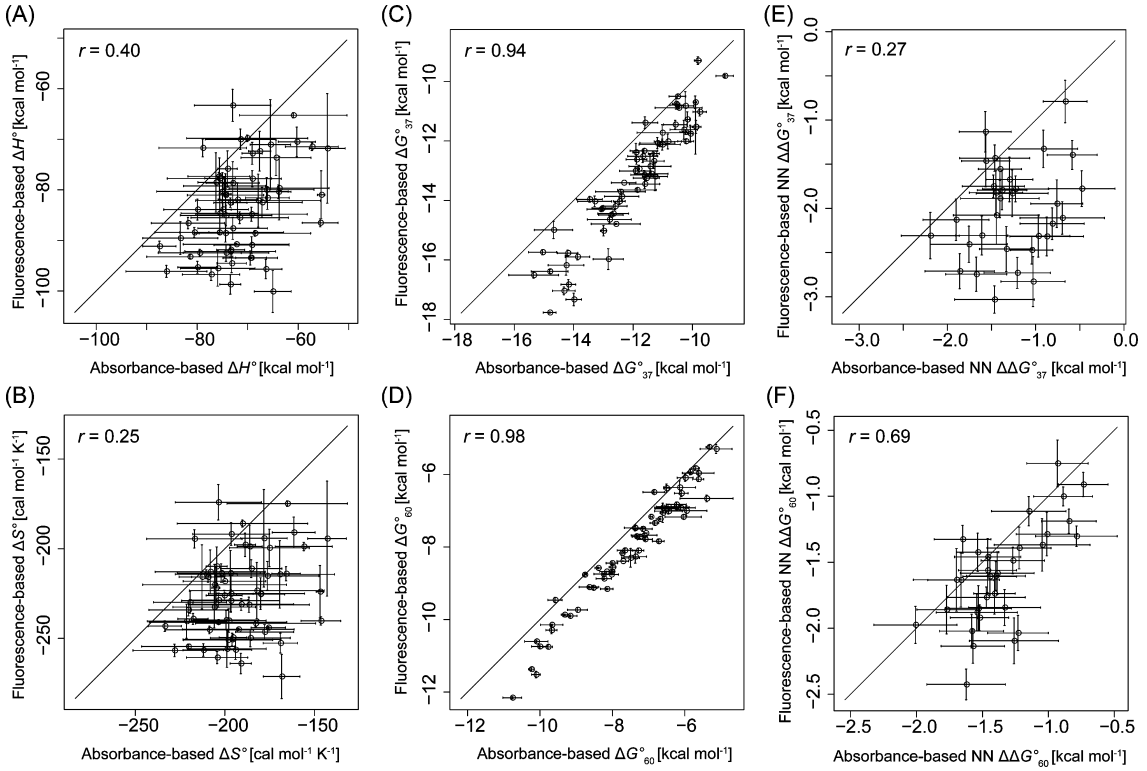

Figure 7. Comparison between the absorbance- and fluorescence-based thermodynamic parameters using Pearson correlations. (A) Comparison of ΔH°. (B) Comparison of ΔS°. (C) Comparison of ΔG°_{37}. (D) Comparison of ΔG°_{60}. (E) Comparison of nearest neighbor (NN) parameters of $\Delta\Delta G^\circ_{37}$. (F) Comparison of nearest neighbor (NN) parameters of $\Delta\Delta G^\circ_{60}$. The line indicates $y = x$ in all graphs.

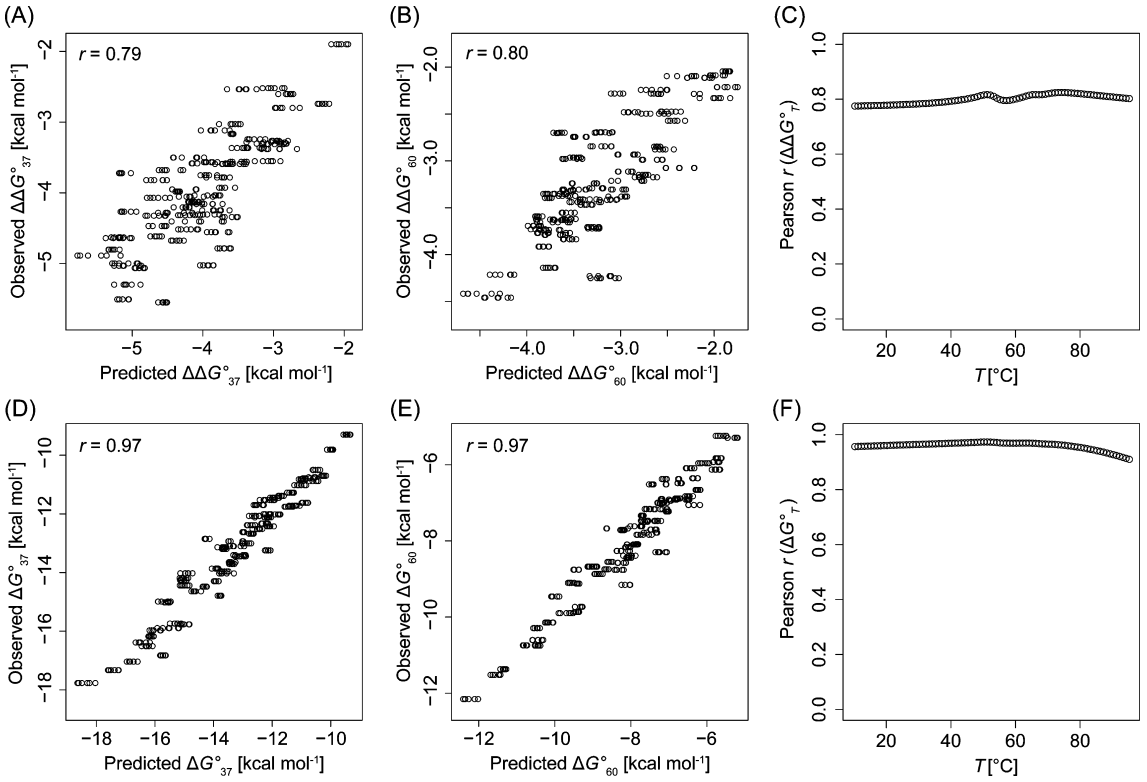

Figure 8. Evaluation of the nearest neighbor thermodynamic parameters derived from the fluorescence melting curves. Comparison between the predicted and observed $\Delta\Delta G^\circ_{37}$ (A), $\Delta\Delta G^\circ_{60}$ (B), ΔG°_{37} (D), and ΔG°_{60} (E). (C and F) Pearson correlation r of the predicted vs observed $\Delta\Delta G^\circ_T$ (C) and ΔG°_T (F) over the temperature range.

dx.doi.org/10.1021/bi300293d | *Biochemistry* 2012, 51, 6056−6067

Table 3. Evaluation with 20-mer Oligonucleotides

ECHO sequence (5′ to 3′)	$\Delta\Delta G^\circ_{37}$ (kcal mol^{-1})		$\Delta\Delta G^\circ_{60}$ (kcal mol^{-1})	
	predicted	observed	predicted	observed
AATATGCGGACT^{E}AAATATAC	−3.0 ± 0.6	−2.5 ± 0.2	−3.1 ± 0.4	−3.8 ± 0.2
TTATGTGTGGT^{E} CGCTTAATA	−1.4 ± 0.6	−1.7 ± 0.5	−2.7 ± 0.4	−2.9 ± 0.5
ATTATGCTCCAAT^{E}CATGTCG	−2.3 ± 0.6	−3.4 ± 0.5	−2.6 ± 0.4	−3.4 ± 0.5

the 20-mer sequences are listed in Table 3. They were in overall agreement, where half of the $\Delta\Delta G^\circ_{37}$ and $\Delta\Delta G^\circ_{60}$ values were within one standard deviation of the predicted values and the rest were within two standard deviations. Therefore, we assume that there is no length effect for predicting relevant thermodynamic parameters of ECHO/DNA duplexes. The approximate incremental free energy can be calculated from the averaged $\Delta\Delta G^\circ_T$ thermodynamic parameters in Table 1 by

$$\Delta\Delta G^\circ_T \approx -2.7 \text{ kcal mol}^{-1} \quad (10)$$

$$\Delta G^\circ_{T(\text{ECHO/DNA})} \approx \Delta G^\circ_{T(\text{DNA/DNA})} - 2.7 \text{ kcal mol}^{-1} \quad (11)$$

This value can be used for rough estimation of the free energy for ECHO/DNA duplex formation.

CONCLUSIONS

Here we have analyzed the thermodynamic parameters of ECHO/DNA duplex formation using a comprehensive set of 64 ECHO/DNA pairs to establish a nearest neighbor model. This model describes the thermodynamic influence of $\mathbf{T}^{\mathbf{E}}$ on DNA/DNA duplex formation. Cross validation tests proved the reliability of our prediction tool for designing ECHOs with $\mathbf{T}^{\mathbf{E}}$ in a central position. Our online tool offers predictions of ECHO/DNA duplex stability at given salt concentrations, helping users to find optimal ECHOs and application conditions for their hybridization and amplification experiments.

ASSOCIATED CONTENT

Supporting Information

Tables and figures summarizing the thermodynamic parameters derived from the fluorescence melting curves. This material is available free of charge via the Internet at http://pubs.acs.org.

AUTHOR INFORMATION

Corresponding Author

*E-mail: y-kimura@gsc.riken.jp. Phone: +81-45-503-9172.

Author Contributions

Y.K. and T.H. contributed equally to this work.

Funding

This work was supported by research grants from the Japanese Ministry of Education, Culture, Sports, Science and Technology (MEXT) for RIKEN Omics Science Center to Y.H., strategic programs for R&D (President's Discretionary Fund) of RIKEN, and a Grant-in-Aid for Scientific Research to A.L.

Notes

The authors declare no competing financial interest.

ACKNOWLEDGMENTS

We acknowledge Toshihisa Ishikawa, Yasushi Kogo, and Alexander Burroughs for helpful comments on the manuscript.

ABBREVIATIONS

$\mathbf{T}^{\mathbf{E}}$, thymidine covalently labeled by two paired thiazole orange molecules; ECHO, exciton-controlled hybridization-sensitive fluorescent oligonucleotide; $\Delta\Delta H^\circ$, $\Delta\Delta S^\circ$, $\Delta\Delta G^\circ_{37}$, $\Delta\Delta G^\circ_{60}$, and ΔT_M, incremental thermodynamic changes caused by a $\mathbf{T}^{\mathbf{E}}$ substitution.

REFERENCES

(1) Southern, E. M. (1975) Detection of specific sequences among DNA fragments separated by gel electrophoresis. *J. Mol. Biol. 98*, 503−517.

(2) Alwine, J. C., Kemp, D. J., and Stark, G. R. (1977) Method for detection of specific RNAs in agarose gels by transfer to diazobenzyloxymethyl-paper and hybridization with DNA probes. *Proc. Natl. Acad. Sci. U.S.A. 74*, 5350−5354.

(3) Volpi, E. V., and Bridger, J. M. (2008) FISH glossary: An overview of the fluorescence in situ hybridization technique. *BioTechniques 45*, 385−386 , 388, 390.

(4) Bilitewski, U. (2009) DNA microarrays: An introduction to the technology. *Methods Mol. Biol. 509*, 1−14.

(5) Wong, M. L., and Medrano, J. F. (2005) Real-time PCR for mRNA quantitation. *BioTechniques 39*, 75−85.

(6) Espy, M. J., Uhl, J. R., Sloan, L. M., Buckwalter, S. P., Jones, M. F., Vetter, E. A., Yao, J. D. C., Wengenack, N. L., Rosenblatt, J. E., Cockerill, F. R., and Smith, T. F. (2006) Real-time PCR in clinical microbiology: Applications for routine laboratory testing. *Clin. Microbiol. Rev. 19*, 165−256.

(7) Tyagi, S., and Kramer, F. R. (1996) Molecular beacons: Probes that fluoresce upon hybridization. *Nat. Biotechnol. 14*, 303−308.

(8) Livak, K. J., Flood, S., Marmaro, J., Giusti, W., and Deetz, K. (1995) Oligonucleotides with fluorescent dyes at opposite ends provide a quenched probe system useful for detecting PCR product and nucleic acid hybridization. *Genome Res. 4*, 357.

(9) Didenko, V. V. (2001) DNA probes using fluorescence resonance energy transfer (FRET): Designs and applications. *BioTechniques 31*, 1106−1116 , 1118, 1120−1121.

(10) Majlessi, M., Nelson, N. C., and Becker, M. M. (1998) Advantages of 2′-O-methyl oligoribonucleotide probes for detecting RNA targets. *Nucleic Acids Res. 26*, 2224−2229.

(11) Vester, B., and Wengel, J. (2004) LNA (locked nucleic acid): High-affinity targeting of complementary RNA and DNA. *Biochemistry 43*, 13233−13241.

(12) Shakeel, S., Karim, S., and Ali, A. (2006) Peptide nucleic acid (PNA): A review. *J. Chem. Technol. Biotechnol. 81*, 892−899.

(13) Molenaar, C., Marras, S. A., Slats, J. C., Truffert, J. C., Lemaître, M., Raap, A. K., Dirks, R. W., and Tanke, H. J. (2001) Linear 2′ O-methyl RNA probes for the visualization of RNA in living cells. *Nucleic Acids Res. 29*, E89.

(14) Bratu, D. P., Cha, B.-J., Mhlanga, M. M., Kramer, F. R., and Tyagi, S. (2003) Visualizing the distribution and transport of mRNAs in living cells. *Proc. Natl. Acad. Sci. U.S.A. 100*, 13308−13313.

(15) Tyagi, S., and Alsmadi, O. (2004) Imaging native β-actin mRNA in motile fibroblasts. *Biophys. J. 87*, 4153−4162.

(16) Ikeda, S., and Okamoto, A. (2008) Hybridization-sensitive on-off DNA probe: Application of the exciton coupling effect to effective fluorescence quenching. *Chem.—Asian J. 3*, 958−968.

(17) Ikeda, S., Kubota, T., Kino, K., and Okamoto, A. (2008) Sequence dependence of fluorescence emission and quenching of

doubly thiazole orange labeled DNA: Effective design of a hybridization-sensitive probe. *Bioconjugate Chem. 19*, 1719−1725.
(18) Okamoto, A. (2011) ECHO probes: A concept of fluorescence control for practical nucleic acid sensing. *Chem. Soc. Rev. 40*, 5815−5828.
(19) Okamoto, A. (2010) Excitonic interaction: Another photophysical process for fluorescence-controlled nucleic acid sensing. *Chem. Rec. 10*, 188−196.
(20) Ikeda, S., Kubota, T., Yuki, M., and Okamoto, A. (2009) Exciton-controlled hybridization-sensitive fluorescent probes: Multicolor detection of nucleic acids. *Angew. Chem., Int. Ed. 48*, 6480−6484.
(21) Lezhava, A., Ishidao, T., Ishizu, Y., Naito, K., Hanami, T., Katayama, A., Kogo, Y., Soma, T., Ikeda, S., Murakami, K., Nogawa, C., Itoh, M., Mitani, Y., Harbers, M., Okamoto, A., and Hayashizaki, Y. (2010) Exciton Primer-mediated SNP detection in SmartAmp2 reactions. *Hum. Mutat. 31*, 208−217.
(22) Petty, J. T., Bordelon, J. A., and Robertson, M. E. (2000) Thermodynamic Characterization of the Association of Cyanine Dyes with DNA. *J. Phys. Chem. B 104*, 7221−7227.
(23) Jacobsen, J. P., Pedersen, J. B., Hansen, L. F., and Wemmer, D. E. (1995) Site selective bis-intercalation of a homodimeric thiazole orange dye in DNA oligonucleotides. *Nucleic Acids Res. 23*, 753−760.
(24) Hansen, L. F., Jensen, L. K., and Jacobsen, J. P. (1996) Bis-intercalation of a homodimeric thiazole orange dye in DNA in symmetrical pyrimidine-pyrimidine-purine-purine oligonucleotides. *Nucleic Acids Res. 24*, 859−867.
(25) Bethge, L., Singh, I., and Seitz, O. (2010) Designed thiazole orange nucleotides for the synthesis of single labelled oligonucleotides that fluoresce upon matched hybridization. *Org. Biomol. Chem. 8*, 2439−2448.
(26) SantaLucia, J., Allawi, H. T., and Seneviratne, P. A. (1996) Improved nearest-neighbor parameters for predicting DNA duplex stability. *Biochemistry 35*, 3555−3562.
(27) SantaLucia, J. (1998) A unified view of polymer, dumbbell, and oligonucleotide DNA nearest-neighbor thermodynamics. *Proc. Natl. Acad. Sci. U.S.A. 95*, 1460−1465.
(28) SantaLucia, J., and Hicks, D. (2004) The thermodynamics of DNA structural motifs. *Annu. Rev. Biophys. Biomol. Struct. 33*, 415−440.
(29) Sugimoto, N., Honda, K.-i., and Sasaki, M. (1994) Application of the Thermodynamic Parameters of DNA Stability Prediction to Double-Helix Formation of Deoxyribooligonucleotides. *Nucleosides Nucleotides 13*, 1311−1317.
(30) Sugimoto, N., Nakano, S., Yoneyama, M., and Honda, K. (1996) Improved thermodynamic parameters and helix initiation factor to predict stability of DNA duplexes. *Nucleic Acids Res. 24*, 4501−4505.
(31) Gray, D. M. (1997) Derivation of nearest-neighbor properties from data on nucleic acid oligomers. II. Thermodynamic parameters of DNA·RNA hybrids and DNA duplexes. *Biopolymers 42*, 795−810.
(32) Owczarzy, R., Vallone, P. M., Gallo, F. J., Paner, T. M., Lane, M. J., and Benight, A. S. (1997) Predicting sequence-dependent melting stability of short duplex DNA oligomers. *Biopolymers 44*, 217−239.
(33) Xia, T., SantaLucia, J., Burkard, M. E., Kierzek, R., Schroeder, S. J., Jiao, X., Cox, C., and Turner, D. H. (1998) Thermodynamic parameters for an expanded nearest-neighbor model for formation of RNA duplexes with Watson-Crick base pairs. *Biochemistry 37*, 14719−1435.
(34) Mathews, D. H., Sabina, J., Zuker, M., and Turner, D. H. (1999) Expanded sequence dependence of thermodynamic parameters improves prediction of RNA secondary structure. *J. Mol. Biol. 288*, 911−940.
(35) Borer, P. N., Dengler, B., Tinoco, I., and Uhlenbeck, O. C. (1974) Stability of ribonucleic acid double-stranded helices. *J. Mol. Biol. 86*, 843−853.
(36) Wu, P., Nakano, S.-i., and Sugimoto, N. (2003) Temperature dependence of thermodynamic properties for DNA/DNA and RNA/DNA duplex formation. *Eur. J. Biochem. 269*, 2821−2830.
(37) Sugimoto, N., Nakano, S., Katoh, M., Matsumura, A., Nakamuta, H., Ohmichi, T., Yoneyama, M., and Sasaki, M. (1995) Thermodynamic parameters to predict stability of RNA/DNA hybrid duplexes. *Biochemistry 34*, 11211−11216.
(38) Griffin, T. J., and Smith, L. M. (1998) An approach to predicting the stabilities of peptide nucleic acid:DNA duplexes. *Anal. Biochem. 260*, 56−63.
(39) Kierzek, E., Mathews, D. H., Ciesielska, A., Turner, D. H., and Kierzek, R. (2006) Nearest neighbor parameters for Watson-Crick complementary heteroduplexes formed between 2′-O-methyl RNA and RNA oligonucleotides. *Nucleic Acids Res. 34*, 3609−3614.
(40) McTigue, P. M., Peterson, R. J., and Kahn, J. D. (2004) Sequence-dependent thermodynamic parameters for locked nucleic acid (LNA)-DNA duplex formation. *Biochemistry 43*, 5388−5405.
(41) Pasternak, A., Kierzek, E., Pasternak, K., Turner, D. H., and Kierzek, R. (2007) A chemical synthesis of LNA-2,6-diaminopurine riboside, and the influence of 2′-O-methyl-2,6-diaminopurine and LNA-2,6-diaminopurine ribosides on the thermodynamic properties of 2′-O-methyl RNA/RNA heteroduplexes. *Nucleic Acids Res. 35*, 4055−4063.
(42) You, Y., Tataurov, A. V., and Owczarzy, R. (2011) Measuring thermodynamic details of DNA hybridization using fluorescence. *Biopolymers 95*, 472−486.
(43) Bonnet, G., Tyagi, S., Libchaber, A., and Kramer, F. R. (1999) Thermodynamic basis of the enhanced specificity of structured DNA probes. *Proc. Natl. Acad. Sci. U.S.A. 96*, 6171−6176.
(44) De Cian, A., Guittat, L., Kaiser, M., Saccà, B., Amrane, S., Bourdoncle, A., Alberti, P., Teulade-Fichou, M.-P., Lacroix, L., and Mergny, J.-L. (2007) Fluorescence-based melting assays for studying quadruplex ligands. *Methods (San Diego, CA, U.S.) 42*, 183−195.
(45) Rachwal, P. A., and Fox, K. R. (2007) Quadruplex melting. *Methods (San Diego, CA, U.S.) 43*, 291−301.
(46) Saccà, B., Meyer, R., and Niemeyer, C. M. (2009) Temperature-dependent FRET spectroscopy for the high-throughput analysis of self-assembled DNA nanostructures in real time. *Nat. Protoc. 4*, 271−285.
(47) Nangreave, J., Yan, H., and Liu, Y. (2009) Studies of thermal stability of multivalent DNA hybridization in a nanostructured system. *Biophys. J. 97*, 563−571.
(48) Albergo, D. D., Marky, L. A., Breslauer, K. J., and Turner, D. H. (1981) Thermodynamics of $(dG\text{-}dC)_3$ double-helix formation in water and deuterium oxide. *Biochemistry 20*, 1409−1413.
(49) Petersheim, M., and Turner, D. H. (1983) Base-stacking and base-pairing contributions to helix stability: Thermodynamics of double-helix formation with CCGG, CCGGp, CCGGAp, ACCGGp, CCGGUp, and ACCGGUp. *Biochemistry 22*, 256−263.
(50) Research and Development Core Team (2011) *R: A language and environment for statistical computing*, R Foundation for Statistical Computing, Vienna.
(51) Markham, N. R., and Zuker, M. (2008) UNAFold: Software for Nucleic Acid Folding and Hybridization. *Bioinformatics, Volume II: Structure, Function and Applications* (Keith, J. M., Ed.) Vol. *453*.
(52) Petruska, J., and Goodman, M. F. (1995) Enthalpy-entropy compensation in DNA melting thermodynamics. *J. Biol. Chem. 270*, 746−750.
(53) Ratilainen, T., Holmén, A., Tuite, E., Nielsen, P. E., and Nordén, B. (2000) Thermodynamics of sequence-specific binding of PNA to DNA. *Biochemistry 39*, 7781−7791.
(54) Liu, L., and Guo, Q. X. (2001) Isokinetic relationship, isoequilibrium relationship, and enthalpy-entropy compensation. *Chem. Rev. 101*, 673−695.
(55) Petersen, M., and Wengel, J. (2003) LNA: A versatile tool for therapeutics and genomics. *Trends Biotechnol. 21*, 74−81.
(56) Karkare, S., and Bhatnagar, D. (2006) Promising nucleic acid analogs and mimics: Characteristic features and applications of PNA, LNA, and morpholino. *Appl. Microbiol. Biotechnol. 71*, 575−586.
(57) Lutsenko, E., and Bhagwat, A. S. (1999) Principal causes of hot spots for cytosine to thymine mutations at sites of cytosine methylation in growing cells. A model, its experimental support and implications. *Mutat. Res. 437*, 11−20.

(58) von Ahsen, N., Wittwer, C. T., and Schütz, E. (2001) Oligonucleotide melting temperatures under PCR conditions: Nearest-neighbor corrections for Mg^{2+}, deoxynucleotide triphosphate, and dimethyl sulfoxide concentrations with comparison to alternative empirical formulas. *Clin. Chem. 47*, 1956−1961.

(59) Owczarzy, R., Moreira, B. G., You, Y., Behlke, M. A., and Walder, J. A. (2008) Predicting stability of DNA duplexes in solutions containing magnesium and monovalent cations. *Biochemistry 47*, 5336−5353.